Water Science and Engineering, 2009, 2(3): 1-12
doi:10.3882/j.issn.1674-2370.2009.03.001

http://kkb.hhu.edu.cn
e-mail: wse@hhu.edu.cn

Numerical research on flow and thermal transport in cooling pool of electrical power station using three depth-averaged turbulence models

Li-ren YU*[1], Jun YU[2]

1. ESDV (Environmental Software and Digital Visualization), São Carlos 13561-120, Brazil
2. College of Mathematics, State University of Campinas, Campinas 13083-859, Brazil

Abstract: This paper describes a numerical simulation of thermal discharge in the cooling pool of an electrical power station, aiming to develop general-purpose computational programs for grid generation and flow/pollutant transport in the complex domains of natural and artificial waterways. Three depth-averaged two-equation closure turbulence models, $\tilde{k}$ - $\tilde{\varepsilon}$, $\tilde{k}$ - $\tilde{w}$, and $\tilde{k}$ - $\tilde{\omega}$, were used to close the quasi three-dimensional hydrodynamic model. The $\tilde{k}$ - $\tilde{\omega}$ model was recently established by the authors and is still in the testing process. The general-purpose computational programs and turbulence models will be involved in a software that is under development. The SIMPLE (Semi-Implicit Method for Pressure-Linked Equation) algorithm and multi-grid iterative method are used to solve the hydrodynamic fundamental governing equations, which are discretized on non-orthogonal boundary-fitted grids with a variable collocated arrangement. The results calculated with the three turbulence models were compared with one another. In addition to the steady flow and thermal transport simulation, the unsteady process of waste heat inpouring and development in the cooling pool was also investigated.

Key words: *waste heat transport; turbulence two-equation closure; depth-averaged* $\tilde{k}$ - $\tilde{\omega}$ *model; cooling pool*

1 Introduction

Waste heat, a major pollution source, is usually produced in various industrial processes such as electrical power production. Waste heat and other passive masses, such as contaminants, are frequently discharged into natural and artificial waterways whose flows are almost always characterized by the presence of turbulence. Dealing with turbulence problems related to thermal and contaminant discharge is a challenge for scientists and engineers, because of the damaging effect of these problems on our limited water resources and fragile environment. It is important to develop adequate mathematical models, numerical methods, and analytical tools to simulate and predict flow and transport in natural and artificial waterways.

This work was supported by FAPESP (Foundation for Supporting Research in São Paulo State), Brazil, of the PIPE Project (Grant No. 2006/56475-3).
*Corresponding author (e-mail: *lirenyu@yahoo.com*)
Received Jun. 29, 2009; accepted Sep. 11, 2009

Although the significance of modeling turbulent flows and transport phenomena with high precision is clear, the numerical simulation and prediction methods for natural and artificial waterways with complex geometry are still unsatisfactory. This is mainly due to the inherent complexity of the problems that need to be considered. Any successful numerical computation for modeling flow and transport processes depends critically on applicable turbulence models, efficient treatment of geometrical boundaries (banks and islands), suitable algorithms, and general-purpose computational programs with corresponding software.

Flows with horizontal lengths that are much greater than their depths can be considered shallow. Depth-averaged mathematical models are often used in shallow and well-mixed flow modeling, which may also be called quasi three-dimensional modeling or shallow flow modeling, because vertical mixing of turbulence diffusion rather quickly evens out the vertical non-uniformity within a limited water column. However, most of these mathematical models consider the turbulent viscosity and diffusivity through constants or merely through simple phenomenological algebraic formulas (Choi and Takashi 2000; Lunis et al. 2004), which are to a great degree estimated according to the modeler's experience. In fact, the turbulent viscosity, relating the Reynolds stresses to the mean velocity gradients, is not a fluid property but strongly depends on the state of turbulence. The turbulence eddy viscosity may vary significantly from one point in the flow to another and also from flow to flow (Rodi 1980).

From an engineering perspective, two-equation closure models can establish a higher standard for numerical approximation of main flow behaviors and transport phenomena in terms of efficiency, extensibility, and robustness (Yu and Righetto 1998, 2001). However, the most common standard two-equation closure models, used widely by various industrial departments, cannot be directly employed in depth-averaged modeling. The depth-averaged versions of corresponding turbulence models should be established in advance. The first two-equation model for depth-averaged calculation was the depth-averaged $\tilde{k}$ - $\tilde{\varepsilon}$ model, suggested by McGuirk and Rodi (1977). In 1989, the first author of the present paper and his colleague also developed a depth-averaged second-order closure model (Yu and Zhang 1989), $\tilde{k}$ - $\tilde{w}$, which originated from the revised k - w model developed by Ilegbusi and Spalding (1982). The k - w model is itself a revised version of an earlier k - ω model, developed in 1969 (Spalding 1969). Many computations have been performed with the $\tilde{k}$ - $\tilde{\varepsilon}$ and $\tilde{k}$ - $\tilde{w}$ models (Rastogi and Rodi 1978; Rodi et al. 1980; Yu 1991; Yu and Righetto 1998, 2001; Yu and Salvador 2005; Yu et al. 2007). However, such examples hardly exist for the simulation of thermal transport in cooling pools with different depth-averaged two-equation turbulence models.

On the other hand, recent advancements in grid generation techniques and numerical methods have provided many suitable approaches, such as non-orthogonal boundary-fitted coordinates and the collocated grid and multi-grid iterative method (Ferziger and Peric 2002). This paper describes a quasi three-dimensional hydrodynamic simulation of flow and thermal transport in a complex multiple-connection domain, with the aim of developing the *grid-generator* and *flow-solver* computational programs and the corresponding numerical tool

(software), which will be used for modeling quasi three-dimensional refined flow and transport phenomena in various complex natural and artificial waterways.

2 Hydrodynamic fundamental governing equations

Depth-averaged mathematical models are frequently used by researchers and engineers for modeling regions with shallow and well-mixed water flow. A typical control volume (CV) is shown in Fig. 1, where *P* is the central node of the CV; *e*, *s*, *w*, and n' are the central nodes of the eastern, southern, western, and northern faces, respectively; *se*, *sw*, *nw*, and *ne* are the four corner points; *E*, *S*, *W*, and *N* are the central nodes of the eastern, southern, western, and northern CVs, respectively; *SE* and *NW* are the central nodes of southeastern and northwestern CVs, respectively; ξ and η are the local coordinates; and i_ξ and i_η are the unit vectors on corresponding coordinates. The integral form of the fundamental governing equations, using vertical Leibniz integration for a CV, considering the variation of the bottom topography and water surface and neglecting minor terms in the depth-averaging procedure, can be written as follows:

$$\frac{\partial}{\partial t}\int_\Omega \rho h\overline{\phi}\,\mathrm{d}\Omega + \int_S \rho h\overline{\phi}\boldsymbol{v}\cdot\boldsymbol{n}\mathrm{d}S = \int_S \Gamma h\mathbf{grad}\overline{\phi}\cdot\boldsymbol{n}\mathrm{d}S + \int_\Omega \overline{q}_\phi \mathrm{d}\Omega \tag{1}$$

where Ω is the CV's volume; S is the face; $\boldsymbol{v}$ is the depth-averaged velocity vector, the superscript "–" indicates that the value is strictly depth-averaged; $\overline{\phi}$ is any depth-averaged conserved intensive property (for mass conservation, $\overline{\phi}=1$; for momentum conservation, $\overline{\phi}$ is the components in different directions of $\boldsymbol{v}$; for conservation of a scalar, $\overline{\phi}$ is the conserved property per unit mass); Γ is the diffusivity for the quantity $\overline{\phi}$; $\overline{q}_\phi$ denotes the source or sink of $\overline{\phi}$; and h and ρ are local water depth and density, respectively. The $\overline{\phi}$ gradient at the center of the cell is expressed through derivatives in global Cartesian coordinates (x, y) or local orthogonal coordinates (n, t):

$$\mathbf{grad}\overline{\phi} = \frac{\partial\overline{\phi}}{\partial x}\boldsymbol{i} + \frac{\partial\overline{\phi}}{\partial y}\boldsymbol{j} = \frac{\partial\overline{\phi}}{\partial n}\boldsymbol{n} + \frac{\partial\overline{\phi}}{\partial t}\boldsymbol{t} \tag{2}$$

where $\boldsymbol{i}$ and $\boldsymbol{j}$ are the unit vectors; and $\boldsymbol{n}$ and $\boldsymbol{t}$ are the unit vectors in the coordinate directions normal and tangential to the face, respectively.

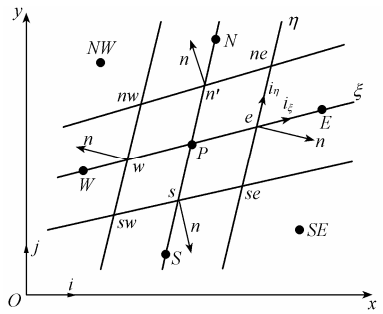

Fig. 1 Typical control volume

For the momentum conservation of Eq. (1), $\Gamma = \tilde{\mu}_{\text{eff}}$ (depth-averaged effective viscosity); for temperature or concentration transport, $\Gamma = \tilde{\Gamma}_{\phi,\text{t}}$ (temperature or concentration diffusivity), where the superscript "~" indicates the quantity characterizing depth-averaged turbulence. The source (sink) term $\overline{q}_\phi$ for momentum conservation may include surface wind shear stresses, bottom shear stresses, pressure terms and additional point sources (or point sinks). The local water depth h is equal to $z - z_{\text{b}}$, where z and z_{b} are the elevations of the water surface and the bottom, respectively. The difference between h and the local static water depth h_{s} is Δh. It should be noted that the local water depth h in Eq. (1) is usually a variable of position in steady flow and of both time and position in unsteady flow.

The dimensionless continuity and momentum equations as well as the transport equation of the scalar $\overline{\phi}$ in Cartesian coordinates can be expressed as (Yu and Giorgetti 2000)

$$\frac{\partial(\rho h)}{\partial t} + \frac{\partial(\rho h\overline{u})}{\partial x} + \frac{\partial(\rho h\overline{v})}{\partial y} = 0 \tag{3}$$

$$\frac{\partial(\rho h\overline{u})}{\partial t} + \frac{\partial(\rho h\overline{u}^2)}{\partial x} + \frac{\partial(\rho h\overline{u}\overline{v})}{\partial y} = -h\frac{\partial(\rho g\Delta h)}{\partial x} + 2\frac{\partial}{\partial x}\left(\frac{\tilde{\mu}_{\text{eff}}h}{Re}\frac{\partial\overline{u}}{\partial x}\right) + \frac{\partial}{\partial y}\left[\frac{\tilde{\mu}_{\text{eff}}h}{Re}\left(\frac{\partial\overline{u}}{\partial y} + \frac{\partial\overline{v}}{\partial x}\right)\right] + \tau_{\text{sx}} - \tau_{\text{bx}} + \overline{S}_{\text{mx}} \tag{4}$$

$$\frac{\partial(\rho h\overline{v})}{\partial t} + \frac{\partial\rho(h\overline{u}\overline{v})}{\partial x} + \frac{\partial(\rho h\overline{v}^2)}{\partial y} = -h\frac{\partial(\rho g\Delta h)}{\partial y} + 2\frac{\partial}{\partial y}\left(\frac{\tilde{\mu}_{\text{eff}}h}{Re}\frac{\partial\overline{v}}{\partial y}\right) + \frac{\partial}{\partial x}\left[\frac{\tilde{\mu}_{\text{eff}}h}{Re}\left(\frac{\partial\overline{u}}{\partial y} + \frac{\partial\overline{v}}{\partial x}\right)\right] + \tau_{\text{sy}} - \tau_{\text{by}} + \overline{S}_{\text{my}} \tag{5}$$

$$\frac{\partial(\rho h\overline{\phi})}{\partial t} + \frac{\partial(\rho h\overline{u}\overline{\phi})}{\partial x} + \frac{\partial(\rho h\overline{v}\overline{\phi})}{\partial y} = \frac{\partial}{\partial x}\left[\frac{\tilde{\Gamma}_{\phi,\text{t}}h}{Re}\frac{\partial\overline{\phi}}{\partial x}\right] + \frac{\partial}{\partial y}\left[\frac{\tilde{\Gamma}_{\phi,\text{t}}h}{Re}\frac{\partial\overline{\phi}}{\partial y}\right] + \overline{S}_\phi \tag{6}$$

where $\overline{u}$ and $\overline{v}$ are the depth-averaged velocity components in the x and y directions, respectively; Re and g are the Reynolds number and gravity acceleration, respectively; $\overline{S}_{\text{mx}}$, $\overline{S}_{\text{my}}$, and $\overline{S}_\phi$ are source/sink terms; and τ_{sx}, τ_{sy}, τ_{bx}, and τ_{by} are the surface wind shear stresses and bottom shear stresses in the x and y directions. The surface wind shear stresses can be calculated with the following formulas:

$$\tau_{\text{sx}} = C_{\text{d}}\rho_{\text{a}}W^2\cos\alpha, \quad \tau_{\text{sy}} = C_{\text{d}}\rho_{\text{a}}W^2\sin\alpha \tag{7}$$

where ρ_{a} is air density and α is the angle between the wind direction and the x axis. When wind velocity $W < 10$ m/s, the dimensionless wind stress coefficient $C_{\text{d}} \approx 0.9\times10^{-3}$. However, when $W \geq 10$ m/s, $C_{\text{d}} \approx 2.9\times10^{-3}$. The bottom shear stresses can be calculated with the following expressions:

$$\tau_{\text{bx}} = C_{\text{f}}\rho\overline{u}\sqrt{\overline{u}_x^{\,2} + \overline{u}_y^{\,2}}, \quad \tau_{\text{by}} = C_{\text{f}}\rho\overline{v}\sqrt{\overline{u}_x^{\,2} + \overline{u}_y^{\,2}} \tag{8}$$

where the empirical friction factor C_{f} is related to Chezy's coefficient C as follows:

$$C_{\text{f}} = g/C^2 \tag{9}$$

3 Depth-averaged closure turbulence models

The depth-averaged effective viscosity $\tilde{\mu}_{\text{eff}}$ and diffusivity $\tilde{\Gamma}_{\phi,\text{t}}$, which appeared in Eq. (1), are dependent on the molecular dynamic viscosity μ and depth-averaged dynamic viscosity of turbulence $\tilde{\mu}_{\text{t}}$: $\tilde{\mu}_{\text{eff}} = \mu + \tilde{\mu}_{\text{t}}$ and $\tilde{\Gamma}_{\phi,\text{t}} = \tilde{\mu}_{\text{t}} / \sigma_{\phi,\text{t}}$, where $\sigma_{\phi,\text{t}}$ is the turbulence Prandtl/Schmidt number for temperature/concentration diffusion, and $\tilde{\mu}_{\text{t}}$ can be determined by two extra turbulence parameters.

For the $\tilde{k}$ - $\tilde{\varepsilon}$ model, the depth-averaged dynamic viscosity $\tilde{\mu}_{\text{t}}$ can be expressed as $\tilde{\mu}_{\text{t}} = \rho C_{\mu} \tilde{k}^2 / \tilde{\varepsilon}$, where C_{μ} is an empirical constant, and $\tilde{k}$ and $\tilde{\varepsilon}$ are determined by solving two extra turbulence parameter transport equations (the $\tilde{k}$ equation and $\tilde{\varepsilon}$ equation). However, $\tilde{\mu}_{\text{t}}$ in the $\tilde{k}$ - $\tilde{w}$ model is defined as $\tilde{\mu}_{\text{t}} = \rho \tilde{k}^2 / \tilde{w}^{1/2}$, and the turbulence parameter equations (the $\tilde{k}$ equation and $\tilde{w}$ equation) should be solved in this model as well.

Recently, the authors have established a new depth-averaged model, $\tilde{k}$ - $\tilde{\omega}$, based on the most common standard k - ω model (in which ω is the special dissipation rate), originally introduced by Saffman but popularized by Wilcox (1998). Assuming the local depth-averaged turbulence in well-mixed shallow waterways is represented by the turbulence kinetic energy $\tilde{k}$ and special dissipation rate of turbulence kinetic energy $\tilde{\omega}$ in the depth-averaged sense, the depth-averaged dynamic viscosity of turbulence $\tilde{\mu}_{\text{t}} = \rho \tilde{k} / \tilde{\omega}$, where $\tilde{k}$ and $\tilde{\omega}$ are determined in terms of the two following coordinate-free vector forms of turbulence parameter transport equations:

$$\frac{\partial(\rho h \tilde{k})}{\partial t} + \text{div}\left(\rho h \tilde{k} \mathbf{v}\right) = \text{div}\left[h\left(\mu + \frac{\tilde{\mu}_{\text{t}}}{\sigma_k^*} \right) \mathbf{grad} \tilde{k} \right] + hP_k - \rho \beta^* h \tilde{k} \tilde{\omega} + \rho h P_{kv} + \overline{S}_k \tag{10}$$

$$\frac{\partial(\rho h \tilde{\omega})}{\partial t} + \text{div}\left(\rho h \tilde{\omega} \mathbf{v}\right) = \text{div}\left[h\left(\mu + \frac{\tilde{\mu}_{\text{t}}}{\sigma_\omega^*} \right) \mathbf{grad} \tilde{\omega} \right] + \alpha h \frac{\tilde{\omega}}{\tilde{k}} P_k - \rho h \beta \tilde{\omega}^2 + \rho h P_{\omega v} + \overline{S}_\omega \tag{11}$$

where $\overline{S}_k$ and $\overline{S}_\omega$ are the source/sink terms, and P_k is the production of turbulent kinetic energy due to interactions of turbulent stresses with horizontal mean velocity gradients. In Cartesian coordinates, Eqs. (10) and (11) can be expressed as follows:

$$\frac{\partial(\rho h \tilde{k})}{\partial t} + \frac{\partial(\rho h \overline{u}_j \tilde{k})}{\partial x_j} = hP_k - \rho \beta^* h \tilde{k} \tilde{\omega} + \frac{\partial}{\partial x_j}\left[\left(\mu + \frac{\tilde{\mu}_{\text{t}}}{\sigma_k^*} \right) h \frac{\partial \tilde{k}}{\partial x_j} \right] + \rho h P_{kv} + \overline{S}_k \tag{12}$$

$$\frac{\partial(\rho h \tilde{\omega})}{\partial t} + \frac{\partial(\rho h \overline{u}_j \tilde{\omega})}{\partial x_j} = \alpha h \frac{\tilde{\omega}}{\tilde{k}} P_k - \rho h \beta \tilde{\omega}^2 + \frac{\partial}{\partial x_j}\left[\left(\mu + \frac{\tilde{\mu}_{\text{t}}}{\sigma_\omega^*} \right) h \frac{\partial \tilde{\omega}}{\partial x_j} \right] + \rho h P_{\omega v} + \overline{S}_\omega \tag{13}$$

where

$$P_k = \tilde{\mu}_{\text{t}} \left[2\left(\frac{\partial \overline{u}}{\partial x} \right)^2 + 2\left(\frac{\partial \overline{v}}{\partial y} \right) + \left(\frac{\partial \overline{u}}{\partial y} + \frac{\partial \overline{v}}{\partial x} \right)^2 \right] \tag{14}$$

The values of empirical constants α, β, β^*, σ_k^*, and σ_ω^* in Eqs. (10) through (13) are the same as in the standard k - ω model: 5/9, 0.075, 0.9, 2, and 2, respectively. The additional source term P_{kv} in the k equation stands for $C_k u_*^3 / h$, where $C_k = 1/\sqrt{C_{\text{f}}}$ and u_* is friction

velocity. According to the dimensional analysis, $P_{\omega v} = C_\omega u_*^2 / h^2$ in Eq. (13), while C_ω is generally $10.89/\sqrt{C_\mathrm{f}}$ for open channels and $1.39/\sqrt{C_\mathrm{f}}$ for natural rivers.

4 Grid generation

A Graphical User Interface (GUI) was developed. It can help the user easily prepare the file needed by the *grid-generator* program for solution in either simple connected domains or multiple-connection domains (Yu and Yu 2008). The interface possesses a self-contained map-support tool, which can be used in various Windows-based microcomputers.

The computational domain of this simulation had strongly curved C-type sides and contained an island, shown in Fig. 2, with detailed bottom topography data. The map scale was 1:30 000 and the water surface elevation was 145.0 m. In the computation, the boundaries of the cooling pool and the island were approximated with a series of short broken lines. Hence, the pool was divided into 82 pieces in the geographic data collection process using the developed GUI (Fig. 3). There were two grid levels and the total length of the pool was around 7.129 km. A file was created by the *grid-generator*, in which the grid data needed by the *flow-solver* were written. Also, postscript files showing the grid of each level were created. Fig. 4 and Fig. 5 show the generated non-orthogonal boundary-fitted coarse grid and fine grid, where the transversal grid nodes are uniform. The three parameters used to determine the island localization in the coarse grid, the CV's numbers from the inlet to the beginning of the island, from the inlet to the end of the island, and from the south side of the pool to the southern boundary of the island, were 90, 103 and 18, respectively. The island's boundaries were divided into 13 pieces. The resolutions of the coarse grid and the fine grid were 177 × 26 and 352 × 50, respectively.

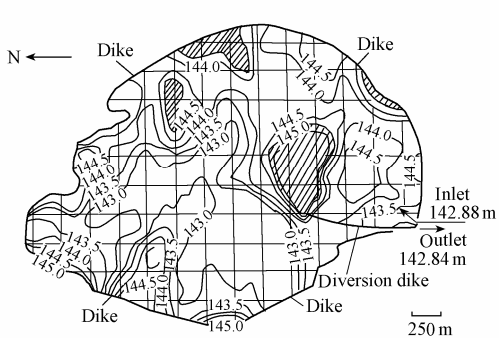

Fig. 2 Pool configuration(unit: m)

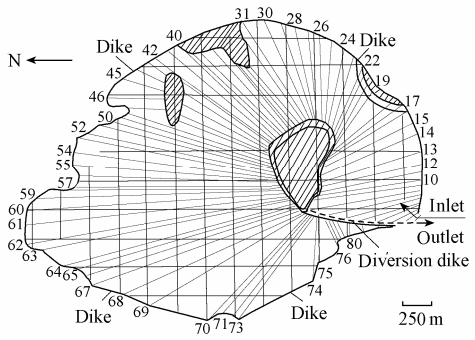

Fig. 3 Multiple-connection domain drawn by GUI

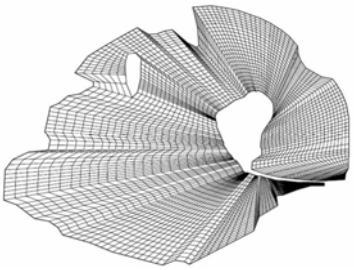

Fig. 4 Coarse grid

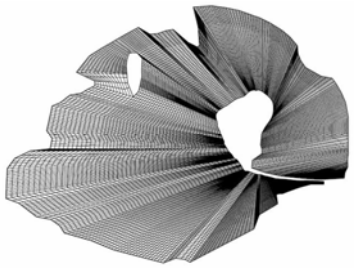

Fig. 5 Fine grid

5 Solutions of flow and thermal discharge

The depth-averaged flow behaviors and temperature distributions were calculated using the developed *flow-solver*, which adopts the SIMPLE (Semi-Implicit Method for Pressure-Linked Equation) algorithm for the FVA (Finite Volume Approach), ILU (Incomplete Lower-Upper) decomposition, the PWIM (Pressure Weighting Interpolation Method), the SIP (Strongly Implicit Procedure), and the relaxation and multi-grid iterative method. The flow rate of cooling water was 30.6 m^3/s, while the friction factor (C_f) was 0.002. The inlet, outlet, and environmental temperatures were 33.2℃, 24.5℃, and 17.8℃, respectively. Using empirical formulas with the mean velocity at the inlet section U_0 = 0.27 m/s, the turbulence parameters of the same section were calculated; parameters $\tilde{k}_0$, $\tilde{\varepsilon}_0$, $\tilde{w}_0$, and $\tilde{\omega}_0$ were 0.02 m^2/s^2, 2×10^{-5} m^2/s^3, 0.03 m/s^2, and 0.12 s^{-1}, respectively. The bottom topography data corresponding to a coarse grid were prepared using the GUI, and thus could be read by the *flow-solver*. The wall function approximation was used to determine the values of velocity components and turbulence parameters at the nodal points in the vicinity of pool banks and island boundaries. In this computation, the momentum equations, pressure-correction equation, and turbulence parameter transport equations of the grid for each level were iteratively solved first, and the fine grid temperature transport equation was solved afterwards. The surface wind's effect on the computation was neglected and the heat diffusion coefficient (*K*) of the water surface was calculated using Gunneberg's equation (Gunneberg 1978).

The simulation obtained various fields of flow, pressure, temperature, and turbulent parameters, which are useful for analysis of engineering problems. Figs. 6 through 13 present some of the results calculated using the $\tilde{k}$-$\tilde{\varepsilon}$ model. For the flow pattern, velocity vectors colored according to their magnitude are plotted at the central points of the CV. Twenty-four contour lines are plotted, where the contour levels are calculated between the maximum and minimum values of drawn variables. Fig. 14 and Fig. 15 also illustrate the flow patterns on the fine grid, but show calculation results of the $\tilde{k}$-$\tilde{w}$ and $\tilde{k}$-$\tilde{\omega}$ closure models; they are similar to Fig. 6 (calculated with the $\tilde{k}$-$\tilde{\varepsilon}$ model). Fig. 16 and Fig. 17 show $\tilde{k}$ contours generated by the $\tilde{k}$-$\tilde{w}$ and $\tilde{k}$-$\tilde{\omega}$ models, respectively. They are also similar to Fig. 11 (calculated with the $\tilde{k}$-$\tilde{\varepsilon}$ model). However, the $\tilde{k}$ contours of these three figures (Fig. 11, Fig. 16 and Fig. 17) demonstrate that the values of the $\tilde{k}$ variable calculated with the $\tilde{k}$-$\tilde{\omega}$ model (Fig. 17) are to a certain extent different from those calculated with the other two models. Fig. 18 and Fig. 19 show $\tilde{w}$ and $\tilde{\omega}$ contours. They are quite different from each other and also different from those in Fig. 12 ($\tilde{\varepsilon}$ contours), because of the different definitions of dissipation rates in the three turbulence models. Fig. 20 and Fig. 21 display the $\tilde{\mu}_t$ contours on the fine grid, calculated with the $\tilde{k}$-$\tilde{w}$ and $\tilde{k}$-$\tilde{\omega}$ models, respectively. It is clear that Fig. 20 is quite similar to Fig. 13 (calculated with the $\tilde{k}$-$\tilde{\varepsilon}$ model), but Fig. 21 is a little different from these two figures in its contour level values. The transport properties of the depth-averaged $\tilde{k}$-$\tilde{\omega}$ model may be different from those of the $\tilde{k}$-$\tilde{\varepsilon}$ and $\tilde{k}$-$\tilde{w}$ models.

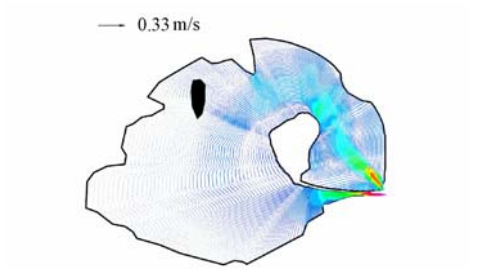

Fig. 6 Flow pattern on fine grid ($\tilde{k}$ - $\tilde{\varepsilon}$)

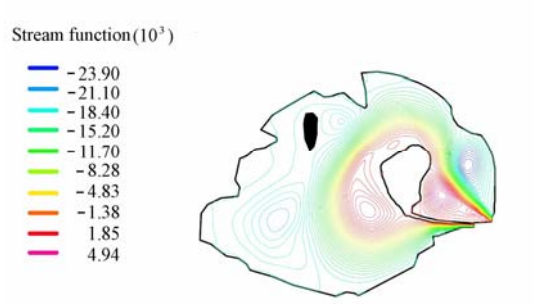

Fig. 7 Streamlines on fine grid ($\tilde{k}$ - $\tilde{\varepsilon}$)

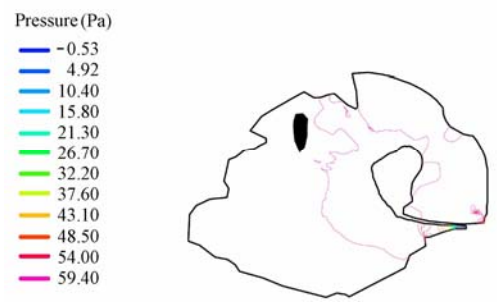

Fig. 8 Isobars on fine grid ($\tilde{k}$ - $\tilde{\varepsilon}$)

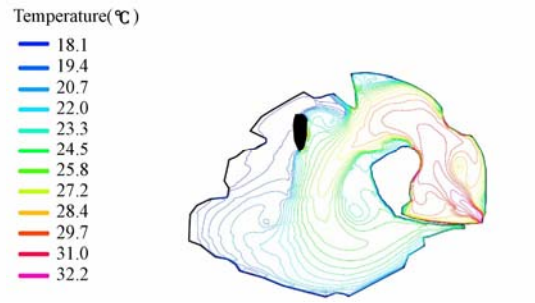

Fig. 9 Isotherms on fine grid ($\tilde{k}$ - $\tilde{\varepsilon}$)

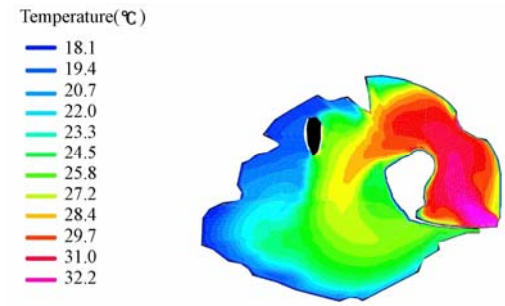

Fig. 10 Temperature distribution on fine grid ($\tilde{k}$ - $\tilde{\varepsilon}$)

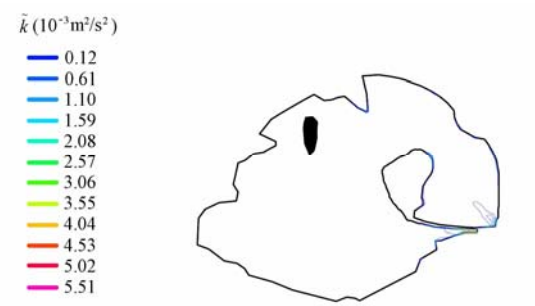

Fig. 11 $\tilde{k}$ contours on fine grid ($\tilde{k}$ - $\tilde{\varepsilon}$)

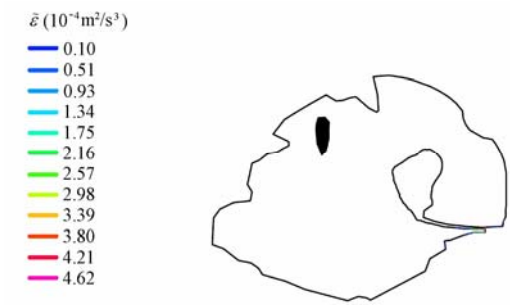

Fig. 12 $\tilde{\varepsilon}$ contours on fine grid ($\tilde{k}$ - $\tilde{\varepsilon}$)

Fig. 13 $\tilde{\mu}_t$ contours on fine grid ($\tilde{k}$ - $\tilde{\varepsilon}$)

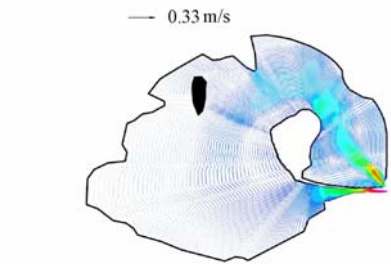

Fig. 14 Flow pattern on fine grid ($\tilde{k}$ - $\tilde{w}$)

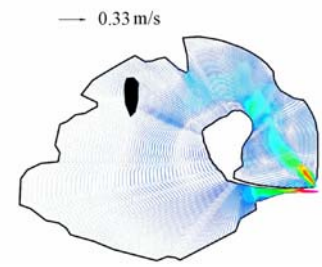

Fig. 15 Flow pattern on fine grid ($\tilde{k}$ - $\tilde{\omega}$)

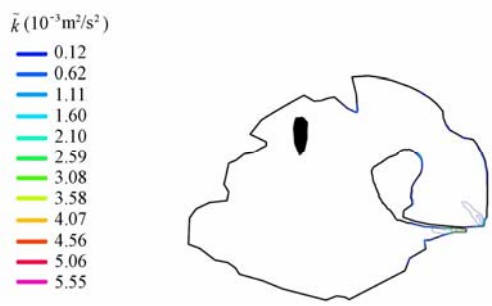

Fig. 16 $\tilde{k}$ contours on fine grid ($\tilde{k}$ - $\tilde{w}$)

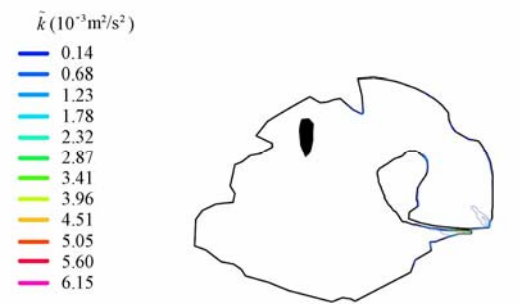

Fig. 17 $\tilde{k}$ contours on fine grid ($\tilde{k}$ - $\tilde{\omega}$)

Fig. 18 $\tilde{w}$ contours on fine grid ($\tilde{k}$ - $\tilde{w}$)

Fig. 19 $\tilde{\omega}$ contours on fine grid ($\tilde{k}$ - $\tilde{\omega}$)

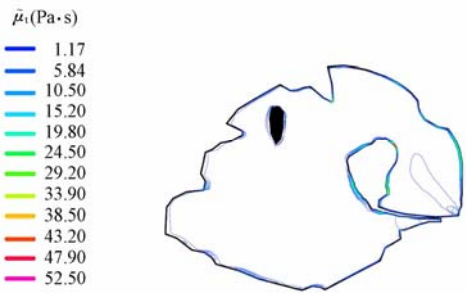

Fig. 20 $\tilde{\mu}_t$ contours on fine grid ($\tilde{k}$ - $\tilde{w}$)

Fig. 21 $\tilde{\mu}_t$ contours on fine grid ($\tilde{k}$ - $\tilde{\omega}$)

Zhang (1988) points out that some expressions of the heat diffusion coefficient (K) commonly used in engineering usually provide a higher value. Hence a special numerical test, controlled by the temperature at the outlet (24.5℃), using Gunneberg's equation to calculate K, and solving the fundamental governing equations with three different turbulence models, was carried out. Fig. 22 presents a comparison of temperature profiles along the centers of the volume cells at j = 7 on the fine grid (i.e., along a curved line from the inlet to the outlet near the inner boundary), calculated by the depth-averaged $\tilde{k}$-$\tilde{\varepsilon}$, $\tilde{k}$-$\tilde{w}$, and $\tilde{k}$-$\tilde{\omega}$ turbulence models. It was found that Gunneberg's equation may also overestimate the heat diffusion coefficient. According to our numerical test, the reduction percentage is 91% for the $\tilde{k}$-$\tilde{\varepsilon}$ and $\tilde{k}$-$\tilde{w}$ models and 92% for the $\tilde{k}$-$\tilde{\omega}$ model.

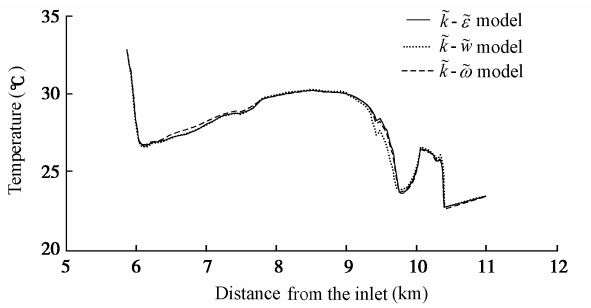

Fig. 22 Comparison of temperature profiles at j = 7 on the fine grid

6 Thermal plume development at beginning of discharge

In order to understand the thermal transport development process, a special simulation was also performed for the following case: the inflow temperature at the inlet is 17.8℃ (environmental temperature) at time t = 0, and then instantaneously becomes 33.2℃ when t > 0, while the flow rate at the inlet remains constant. The hydrodynamic fundamental governing equations of this computation were solved with the depth-averaged $\tilde{k}$-$\tilde{\varepsilon}$ model. Figs. 23(a) through (f) display the depth-averaged temperature field at t = 0, Δt, $2\Delta t$, $3\Delta t$, $4\Delta t$, and $5\Delta t$, respectively.

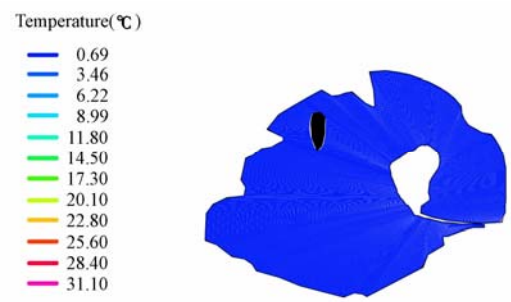

(a) Case 1, t = 0

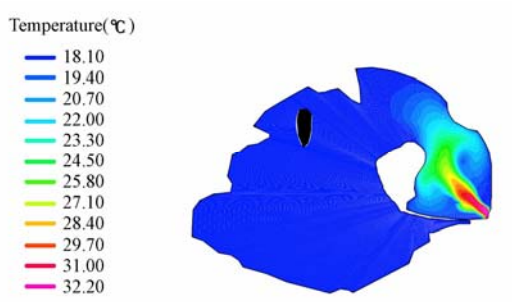

(b) Case 2, $t = \Delta t$

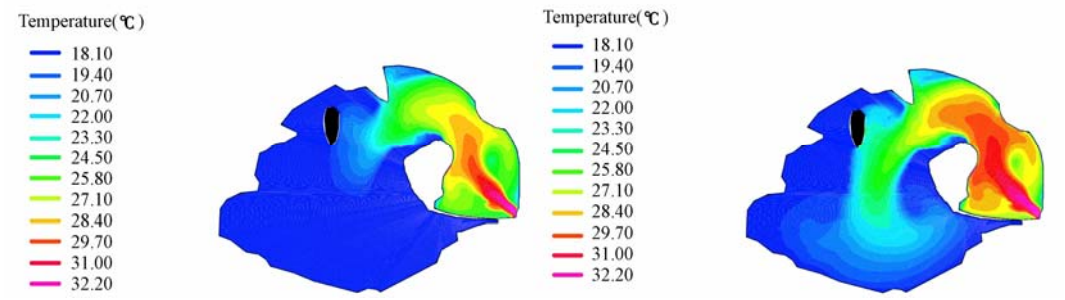

(c) Case 3, $t = 2\Delta t$ (d) Case 4, $t = 3\Delta t$

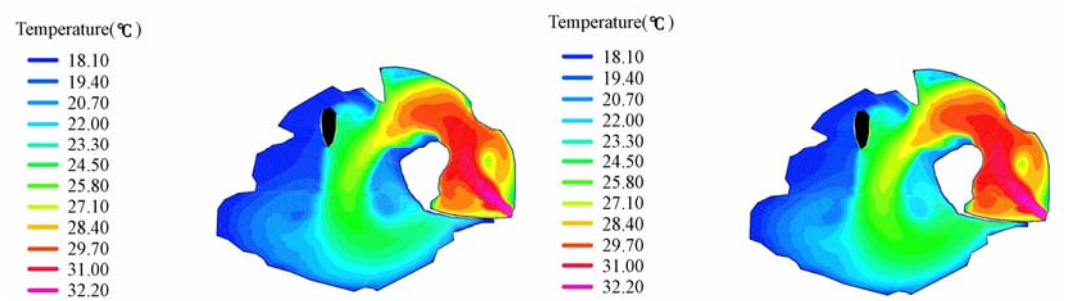

(e) Case 5 $t = 4\Delta t$ (f) Case 6, $t = 5\Delta t$

Fig. 23 Simulated depth-averaged temperature field

7 Discussion and conclusions

The flow and thermal transport in a cooling pool have been simulated using three depth-averaged turbulence models: $\tilde{k}$ - $\tilde{\varepsilon}$, $\tilde{k}$ - $\tilde{w}$, and $\tilde{k}$ - $\tilde{\omega}$. The development process of waste heat discharge has also been numerically investigated. At the same time, a pre-processing GUI and corresponding map-support tool have been developed. Two general-purpose computational programs were created, one for grid generation (*grid-generator*), which possesses the ability to generate multiple grids for complex computational domains, and the other for flow/pollutant transport computation (*flow-solver*), which has the ability to simulate practical problems using advanced two-equation closure models.

The newly established depth-averaged turbulence model, $\tilde{k}$ - $\tilde{\omega}$, was used in the computation along with two existing models ($\tilde{k}$ - $\tilde{\varepsilon}$ and $\tilde{k}$ - $\tilde{w}$). It was proved that the $\tilde{k}$ - $\tilde{\omega}$ model is suitable for shallow water modeling. The overestimation of the heat diffusion coefficient by Gunneberg's equation was also verified. Although the temperature distributions computed by the three depth-averaged turbulence models ($\tilde{k}$ - $\tilde{\varepsilon}$, $\tilde{k}$ - $\tilde{w}$, and $\tilde{k}$ - $\tilde{\omega}$) are in general similar, the properties and abilities of the $\tilde{k}$ - $\tilde{\omega}$ model are to a certain extent different from those of the $\tilde{k}$ - $\tilde{\varepsilon}$ and $\tilde{k}$ - $\tilde{w}$ models. Of course, the behaviors of the depth-averaged $\tilde{k}$ - $\tilde{\omega}$ model should be further investigated.

The thermal plume in the cooling pool is mixed sufficiently in its beginning stage (from the entry to the island). However, due to the horizontal expansion from the island in the lower

reach, engineering approaches may be considered to change the horizontal flow pattern in order to further expand the plume and thus enhance cooling efficiency.

References

Choi, M., and Takashi, H. 2000. A numerical simulation of lake currents and characteristics of salinity changes in the freshening process. *Journal of Japan Society of Hydrology and Water Resources*, 13(6), 439-452. (in Japanese)

Ferziger, J. H., and Peric, M. 2002. *Computational Methods for Fluid Dynamics,* 3rd Edition. Berlin: Springer.

Gunneberg, F. 1978. Problems with the computation of water and atmosphere interfaces. *Warm discharge in waters and their effects. The waste Heat Commission Office at Federal Office for Environment Protection*. Berlin. (in German)

Ilegbusi, J. O., and Spalding, D. B. 1982. *Application of a New Version of the k-w Model of Turbulence to a Boundary Layer with Mass Transfer*, *CFD/82/15*. London: Imperial College.

Lunis, M., Mamchuk, V. I., Movchan, V. T., Romanyuk, L. A., and Shkvar, E. A. 2004. Algebraic models of turbulent viscosity and heat transfer in analysis of near-wall turbulent flows. *International Journal of Fluid Mechanics Research*, 31(3), 60-74. [doi:10.1615/InterJFluidMechRes.v31.i3.60]

McGuirk, J. J., and Rodi, W. 1977. *A Depth-Averaged Mathematical Model for Side Discharges into Open Channel Flow, SFB 80/T/88*. Karlsruhe: Universität Karlsruhe.

Rastogi, A. K., and Rodi, W. 1978. Predictions of heat and mass transfer in open channels. *Journal of the Hydraulics Division*, 104(3), 397-420.

Rodi, W. 1980. Turbulence models for environmental problems. Kollmann, W., ed., *Prediction Methods for Turbulent Flows*, 159-349. Washington: Hemisphere Publishing Corporation.

Rodi, W., Pavlovic, R. N., and Srivatsa, S. K. 1980. Prediction of flow and pollutant spreading in rivers. Fischer, H. B., ed., *Transport Models for Inland and Coastal Waters*: *Proceedings of the Symposium on Predictive Ability*, 63-111. Berkeley: University of California Academic Press.

Spalding, D. B. 1969. *The Prediction of Two-Dimensional, Steady Turbulent Elliptic Flows. Heat Transfer Section Report EF/TN/A/16*. London: Imperial College.

Wilcox, D. C. 1998. *Turbulence Modeling for CFD*. La Canada: DCW Industries, Inc.

Yu, L. R., and Zhang, S. N. 1989. A new depth-averaged two-equation ($\tilde{k}$ - $\tilde{w}$) turbulent closure model. *Journal of Hydrodynamics, Series B*, 1(3), 47-54.

Yu, L. R. 1991. A new depth-averaged two-equation ($\tilde{k}$ - $\tilde{w}$) turbulent closure model and its application to numerical simulation for a river. *Journal of Hydrodynamics, Series B*, 3(2), 21-28.

Yu, L. R., and Righetto, A. M. 1998. Tidal and transport modeling by using turbulence $\tilde{k}$ - $\tilde{w}$ model. *Journal of Environmental Engineering*, 124(3), 212-221. [doi:10.1061/(ASCE)0733-9372(1998)124:3(212)]

Yu, L. R., and Giorgetti, M. F. 2000. Hydrodynamic analysis of flow patterns and estimation of retention time for a polluted reservoir. *Journal of Mechanical Engineering Science*, *Proceedings Part C*, 214(6), 873-880. [doi:10.1243/0954406001523858]

Yu, L. R., and Righetto, A. M. 2001. Depth-averaged turbulence $\tilde{k}$ - $\tilde{w}$ model and applications. *Advances in Engineering Software*, 32(5), 375-394. [doi:10.1016/S0965-9978(00)00100-9]

Yu, L. R., and Salvador, N. N. B. 2005. Flow modeling for natural river. *Proceedings of the 2nd International Yellow River Forum on Keeping Healthy Life of the River, Volume III*, 202-207. Zhengzhou: Yellow River Conservancy Press.

Yu, L. R., Salvador, N. N. B., and Yu, J. 2007. Models, methods and software development of contaminant transport in meandering rivers. *Proceedings of the 3rd International Yellow River Forum on Sustainable Water Resources Management and Delta Ecosystem Maintenance, Volume VI*, 47-56. Zhengzhou: Yellow River Conservancy Press.

Yu, L. R., and Yu, J. 2008. Flow and contaminant transport in a multiply-connected domain of natural river. *Proceedings of the 16th IAHR-APD Congress and 3rd Symposium of IARH-ISHS, Volume II: Environmental and Ecological Hydraulics*, 727-731. Beijing: Tsinghua University Press.

Zhang, S. N. 1988. *Environmental Hydromechanics*. Nanjing: Hohai University Press. (in Chinese)